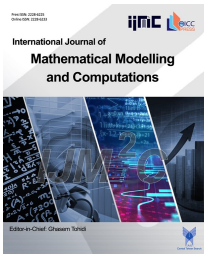

Int. J. Math. Model. Comput. 15(4) (2025) 234-247

International Journal of Mathematical Modelling & Computations (IJM^{2}C)

https://doi.org/10.57647/ijm2c.2025.150423

Solving fractional optimal control problems and costate estimation via a Müntz pseudospectral method

Hussein Ghassemi[1], Mohammad Maleki[2,*]

[1]*Department of Mathematics, Nae. C., Islamic Azad University, Naein, Iran*
[2]*Department of Mathematics, Isf. C., Islamic Azad University, Isfahan, Iran*

[*]**Corresponding author:** mm.maleki2025@iau.ir

Original Research

Received:
09 July 2025
Revised:
05 August 2025
Accepted:
07 August 2025
Published online:
10 August 2025
Published in Issue:
31 Decembre 2025

Abstract:

In this paper, we first introduce the Müntz–Legendre polynomials and establish their relation to Jacobi polynomials. Then, a stable scheme is presented for approximating the Caputo fractional derivative of the Müntz–Legendre polynomials. Next, we introduce a Müntz–polynomial pseudospectral method with fractional power of Legendre–Gauss–Radau mesh points for solving fractional optimal control problems. This method is particularly suitable for problems whose solutions contain non-integer exponent factors. We also construct a novel costate estimation procedure based on the first order optimality conditions and the structure of the underlying problem. Three numerical examples, including a fractional model for tumor burden under immune suppression, are presented to demonstrate the applicability and spectral accuracy of the proposed method.

Keywords: Fractional optimal control; Pseudospectral; Costate estimation; Müntz polynomials; Fractional cancer model.

Cite this article: Ghassemi H, Maleki M. Solving fractional optimal control problems and costate estimation via a M"untz pseudospectral method. *Int J Math Model Comput*. 2025;15(4):234–247.https://doi.org/10.57647/ijm2c.2025.150423

1. Introduction

Orthogonal collocation or pseudospectral (PS) methods lie among direct methods that possesses spectral accuracy for problems having smooth or piecewise smooth solutions. Using state-control parameterization via orthogonal polynomials and collocating the system dynamics at collocation nodes obtained from a Gaussian quadrature, PS methods transcribe an optimal control problem (OCP) to a nonlinear programming problem (NLP).

During the past two decades, PS methods have been extensively used in solving OCPs [1, 2] and in resent years many researchers have tried to extend PS methods to solve various types of fractional optimal control problems (FOCPs) [3–8]. Some other numerical methods have also been developed for solving FOCPs such as indirect spectral Chebyshev and direct Clenshaw–Curtis scheme followed by the Rayleigh–Ritz method [9], indirect spectral method using hybrid functions [10], an iterative approach [11], Variational iteration and modified Adomian decomposition methods [12], a combination of the perturbation homotopy and parameterization methods [13], Bernstein polynomials operational matrices [14], Epsilon–Ritz method [15], Adomian decomposition method [16], indirect convergent Jacobi spectral collocation [17], indirect Chebyshev cardinal functions method [18] and a convergent Legendre spectral collocation method [19].

Further, numerical solution of some applied models using FOCPs has been considered by some authors such as HIV/AIDS epidemic model with random testing and

contact tracing [20], Mosaic disease [21], mathematical model of tumor under immune suppression [22], Cholera epidemic model [23], a Climatic model [24], Hand, Foot and Mouth Disease Model [25] and Hepatitus C virus model [26].

Direct PS methods for OCPs basically do not include a costate estimation scheme; nonetheless, some researchers have developed such schemes for OCPs using the first order optimality conditions [2] or the so called Covector Mapping Principle [27, 28]. For FOCPs, to the best of our knowledge, there is no costate estimation in the literature using direct PS methods. On the other hand, it is well known that spectral methods based on classical polynomials do not have spectral accuracy if the exact solution has a low regularity, as in problems of fractional order. To remedy this deficiency, a way is to utilize nonpolynomials, such as generalized Jacobi functions and Müntz-Legendre polynomials bases [29–31]. Such methods have not been properly developed for FOCPs so far.

Motivating by the above issues, we first introduce a new Müntz PS method for a class of FOCPs. A stable scheme is derived for the numerical computation of Müntz-Legendre polynomials and their Caputo fractional derivative. Then, collocation using fractional power form of Legendre–Gauss-Radau points is done to replace the underlying FOCP to a nonlinear programming problem (NLP). The proposed method possesses the spectral accuracy even for FOCPs with a low regularity. Next, by developing our work in [2] to the fractional case, a novel costate estimation scheme is constructed that utilizes the first order optimality conditions and the Müntz PS approximations of state and control variables.

The remainder of this paper is organized as follows: in Section 2, some preliminaries concerning orthogonal polynomials and fractional calculus are given. Section 3 is devoted to numerical evaluation of Müntz-Legendre polynomials and their Caputo fractional derivative. In Section 4, formulation of the new Müntz PS method is explained and in Section 5 the costate estimation scheme is explored. In Section 6, three illustrative examples, including a tumor burden model under immune suppression, are provided. Finally, conclusions are given in Section 7.

2. Preliminaries

2.1 Nonclassical orthogonal polynomials

Let $w(t)$ represent a non-negative integrable weight function defined on the arbitrary interval $[a, b]$, which establishes the weighted inner or scalar product of the functions $u(t)$ and $v(t)$ by

$$(u, v)_w = \int_a^b u(t)v(t)w(t)dt. \tag{1}$$

It is well known that the weighted scalar product (1) constructs a unique set of orthogonal polynomials $P_k \in \mathbb{P}_k, k = 0, 1, 2, \ldots$, which satisfy a three-term recurrence relation

$$\begin{aligned} P_{k+1}(t) &= (t - \alpha_k)P_k(t) - \beta_k P_{k-1}(t), \qquad (2)\\ P_{-1}(t) &= 0, \qquad P_0(t) = 1, \end{aligned}$$

with the coefficients

$$\alpha_k = \frac{\left(tP_k(t), P_k(t)\right)}{\left(P_k(t), P_k(t)\right)},$$

$$\beta_0 = \left(P_0(t), P_0(t)\right), \qquad \beta_k = \frac{\left(P_k(t), P_k(t)\right)}{\left(P_{k-1}(t), P_{k-1}(t)\right)}.$$

According to Gautschi [32], due to the numerical stability of the recurrence relation (2), it can be effectively utilized for the numerical calculation of orthogonal polynomials. While closed-form expressions for the coefficients of classical orthogonal polynomials are established, the recurrence coefficients for nonclassical weight functions remain unknown. Consequently, numerical methods such as the Stieltjes procedure or the Chebyshev algorithm are employed.

2.2 Jacobi polynomials

Jacobi polynomials, $J_k^{(\alpha,\beta)}(x)$, lie among classical orthogonal polynomials that are defined on the interval $[-1, 1]$ with respect to the weight function $w^{(\alpha,\beta)}(x) = (1-x)^\alpha(1+x)^\beta$ with $\alpha, \beta > -1$. Although they can be obtained using the following closed-form relation:

$$J_k^{(\alpha,\beta)}(x) = \sum_{m=0}^{k} \frac{(-1)^{k-m}(1+\beta)_k(1+\alpha+\beta)_{k+m}}{m!(k-m)!(1+\beta)_m(1+\alpha+\beta)_k}\left(\frac{1+x}{2}\right)^m, \tag{3}$$

where $(d)_0 = 1$ and $(d)_k = d(d+1)\ldots(d+k+1)$, for stability reasons, Jacobi polynomials are evaluated using the following recursive relation [32, 33]:

$$J_0^{(\alpha,\beta)}(x) = 1, J_1^{(\alpha,\beta)}(x) = \frac{1}{2}[(\alpha-\beta)(\alpha+\beta+2)x], \tag{4}$$

$$a_{1,k}^{(\alpha,\beta)}J_{k+1}^{(\alpha,\beta)}(x) = b_{2,k}^{(\alpha,\beta)}J_k^{(\alpha,\beta)}(x) - c_{3,k}^{(\alpha,\beta)}J_{k-1}^{(\alpha,\beta)}(x), \tag{5}$$

where

$$a_{1,k}^{(\alpha,\beta)} = 2(k+1)(k+\alpha+\beta+1)(2k+\alpha+\beta),$$

$$b_{2,k}^{(\alpha,\beta)} = (2k+\alpha+\beta+1).[(2k+\alpha+\beta+1)(2k+\alpha+\beta+2)x],$$

$$c_{3,k}^{(\alpha,\beta)} = c_{3,k}^{(\alpha,\beta)} = 2(k+\alpha)(k+\beta)(2k+\alpha+\beta+2).$$

As well, the recursive relation for calculating the first derivative of Jacobi polynomials is given by

$$\frac{d}{dx}J_k^{(\alpha,\beta)}(x) = \frac{1}{2}(k+\alpha+\beta+1)J_{k-1}^{(\alpha+1,\beta+1)}(x). \tag{6}$$

For more information we refer to [33].

https://doi.org/10.57647/ijm2c.2025.150423

2.3 Gauss quadrature rule

The general form of a numerical quadrature rule with respect to a weight function w is given by

$$\int_a^b f(t)w(t)dt = \sum_{k=1}^{N} w_k f(t_k) + R_N(f), \qquad (7)$$

where N is the number of quadrature points and $R_N(f)$ is the truncation error. This quadrature rule is referred to as a Gauss-type quadrature rule when it becomes precise for polynomials of degree no greater than $2n - l$, where l can take the values 0, 1, or 2. Hopefully, the quadrature nodes t_k and weights w_k corresponding to classical weight functions, such as Jacobi weight functions, are available in tabulated form.

For a nonclassical weight function, however, the algorithm of Golub–Welsch [34] can be used to evaluate the nodes and weights of a Gauss-type quadrature. In this approach by computing the eigenvalues and normalized eigenvectors of the symmetric tridiagonal Jacobi, Jacobi-Lobatto and Jacobi-Radau matrices J^G_{N+1}, J^L_{N+1} and J^R_{N+1} the nodes and weights are determined. Specifically, based on the coefficients given in Eq. (2), the tridiagonal Jacobi matrix of order $N + 1$ is given by

$$J^G_{N+1} = \begin{bmatrix} \alpha_0 & \sqrt{\beta_1} & & & & \\ \sqrt{\beta_1} & \alpha_1 & \sqrt{\beta_2} & & & \\ & \sqrt{\beta_2} & \alpha_2 & \sqrt{\beta_3} & & \\ & & \ddots & & & \\ & & \ddots & & & \\ & & \ddots & & & \\ & & & \sqrt{\beta_{N-1}} & \alpha_{N-1} & \sqrt{\beta_N} \\ & & & & \sqrt{\beta_N} & \alpha_N \end{bmatrix} \qquad (8)$$

Theorem 2.1 *The eigenvalues of J^G_{N+1} are the Gauss nodes $a < t_0 < t_1 < \ldots < t_{N-1} < t_N < b$ and the corresponding quadrature weights $\{w_k\}_{k=0}^N$ are calculated using the formula*

$$w_k = \beta_0(\upsilon_{1k})^2, \qquad k = 1, 2, \ldots, N, \qquad (9)$$

where $\{\upsilon_k\}_{k=0}^N$ represents the normalized eigenvector of J^G_{N+1} associated with the eigenvalue $\{t_k\}_{k=0}^N$ (i.e. $\upsilon_k^T\upsilon_k = 1$) and υ_{1k} denotes its first component.

For more information about the structure of the tridiagonal Jacobi-Lobatto and Jacobi-Radau matrices and corresponding nodes and weights, refer to [34].

2.4 Fractional calculus

Fractional calculus deals with derivatives and integrals of non-integer order and the most popular definitions in fractional calculus refer to the Riemann-Lioville and Caputo definitions [35]. Let $f : [a, b] \to R$ be a function, $\alpha > 0$ be a real number and $m = [\alpha] + 1$. The fractional left and right Riemann-Lioville integrals of order α are respectively defined as follows:

$${}_aI_t^\alpha f(t) = \frac{1}{\Gamma(\alpha)} \int_a^t (t-\tau)^{\alpha-1} f(\tau)d\tau, \quad t > a, \quad (10)$$

$${}_tI_b^\alpha f(t) = \frac{1}{\Gamma(\alpha)} \int_t^b (\tau-t)^{\alpha-1} f(\tau)d\tau, \quad t < b. \quad (11)$$

By using the above fractional integrals, the left Caputo fractional derivative (LCFD) of order α, when it exists, is defined as

$${}_a^C D_t^\alpha f(t) = \frac{1}{\Gamma(m-\alpha)} \int_a^t (t-\tau)^{m-\alpha-1} f^{(m)}(\tau)d\tau, \quad t > a,$$

and the right Caputo fractional derivative (RCFD) is defined as

$${}_t^C D_b^\alpha f(t) = \frac{(-1)^m}{\Gamma(m-\alpha)} \int_t^b (\tau-t)^{m-\alpha-1} f^{(m)}(\tau)d\tau, \quad t < b,$$

where $f^{(m)}(t)$ is the usual m-th derivative of f.

For the Riemann-Lioville fractional integral and Caputo fractional derivative the following properties hold:

$${}_aI_t^\alpha t^k = \frac{\Gamma(k+1)}{\Gamma(k+\alpha+1)} t^{k+\alpha}, \quad t > 0, \qquad (12)$$

and if $k \in \mathbb{N}_0$ and $k > [\alpha]$

$${}_a^C D_t^\alpha t^k = \frac{\Gamma(k+1)}{\Gamma(k-\alpha+1)} t^{k-\alpha}, \quad t > 0. \qquad (13)$$

Moreover, for $0 < \alpha < 1$ we have

$$\begin{aligned} {}_aI_t^\alpha \left({}_a^C D_t^\alpha f(t)\right) &= f(t) - f(a), \qquad (14) \\ {}_tI_b^\alpha \left({}_t^C D_b^\alpha f(t)\right) &= f(t) - f(b). \end{aligned}$$

3. Müntz-Legendre polynomials

Consider the complex sequence $\Lambda_n = \{\lambda_1, \lambda_2, \ldots, \lambda_n\}$ with the property $Re(\lambda_k) > -1$, $k = 1, 2, \ldots, n$. Consider also the following function:

$$w_n(t) = \prod_{k=0}^{n} \frac{t - \overline{\lambda_k} + 1}{t - \lambda_k} \cdot \frac{1}{t - \lambda_n}. \qquad (15)$$

Then, according to [36] the Müntz-Legendre polynomials are defined as

$$L(\Lambda, x) = \frac{1}{2\pi i} \int_C w_n(t) x^t dt. \qquad (16)$$

where C is a simple curve surrounding all the zeros of the denominator in the function $w_n(t)$.

Furthermore, when $\lambda_k \neq \lambda_j$ for $k \neq j$, by using the above definition and the Cauchy residue theorem, the polynomials $L(\Lambda, x)$ can be restated as follows:

$$L_n(t) = L_n(\Lambda_n, t) = \sum_{k=0}^{n} c_{n,k} x^{\lambda_k}, \qquad (17)$$

$$c_{n,k} = \frac{\prod_{\upsilon=0}^{n-1} (\lambda_k + \overline{\lambda_\upsilon} + 1)}{\prod_{\upsilon=0, \upsilon\neq k}^{n} (\lambda_k - \lambda_\upsilon)}.$$

https://doi.org/10.57647/ijm2c.2025.150423

Note that these polynomials are orthogonal on the interval $[0,1]$ with respect to the weight function $w(t)=1$, i.e.

$$(L_i,L_j)=\int_0^1 L_i(x)L_j(x)dx=\frac{\delta_{ij}}{\lambda_k+\overline{\lambda}_k+1}, \quad (18)$$

where $\{\delta_{ij}\}_{i,j=1}^n$ is the Kronecker delta function.

In the special case that $\{\lambda_k=\alpha k\}_{k=1}^n$ (for a positive real number α), by shifting the Müntz polynomials to the interval $I=[0,T]$ we have

$$L_n(t;\alpha)=\sum_{k=0}^{n} C_{n,k}(\frac{t}{T})^{k\alpha}, \quad (19)$$
$$C_{n,k}=\frac{(-1)^{n-k}}{\alpha^n k!(n-k)!}\prod_{k=0}^{n}\Big((k+\upsilon)\alpha+1\Big).$$

They form an orthogonal basis for the space $\mathcal{M}_{n,\alpha}$, where

$$\mathcal{M}_{n,\alpha}=\text{span}\{1,t^\alpha,\ldots,t^{n\alpha}\}.$$

Now, we turn to the numerical calculation of the shifted Müntz-Legendre polynomials and their Caputo fractional derivative. As stated in [30, 37], direct evaluation of these polynomials using the definition (19) can be problematic in finite arithmetic because the coefficients $C_{n,k}$ become very large as n increases. The following theorem adopted from [30], relates the shifted Müntz-Legendre polynomials to a class of Jacobi polynomials.

Theorem 3.1 *For a real number $\alpha>0$ and $t\in I$, we have the following representation:*

$$L_n(t;\alpha)=J_n^{(0,\frac{1}{\alpha}-1)}\left(2\left(\frac{t}{T}\right)^\alpha-1\right). \quad (20)$$

Hence, using the three-term recursive relation (4)–(5) we can obtain $L_n(t;\alpha)$ in a stable manner as follows:

$$L_0(t;\alpha)=1,\quad L_1(t;\alpha)=(\frac{1}{\alpha}+1)\left(\frac{t}{T}\right)^\alpha-\frac{1}{\alpha}, \quad (21)$$

$$b_{1,n}L_{n+1}(t;\alpha)=b_{2,n}(t)L_n(t;\alpha)-b_{3,k}L_{n-1}(t;\alpha), \quad (22)$$

where

$$b_{1,n}=a_{1,n}^{(0,\frac{1}{\alpha}-1)},$$
$$b_{2,n}(t)=a_{2,n}^{(0,\frac{1}{\alpha}-1)}\left(2\left(\frac{t}{T}\right)^\alpha-1\right),$$
$$b_{3,n}=a_{3,n}^{(0,\frac{1}{\alpha}-1)}.$$

Next, for the numerical evaluation of ${}_0^C D_t^\alpha L_n(t;\alpha)$ we have two ways. In the first way, consider again $L_n(t;\alpha)$ as in Eq. (19). By utilizing the well-known formula

$${}_0^C D_t^\alpha t^\beta=\frac{\Gamma(1+\beta)}{\Gamma(1+\beta-\alpha)}t^{\beta-\alpha}, \alpha>0,\beta>-1,t>0, \quad (23)$$

the Caputo derivative of $L_n(t;\alpha)$ can be stated as

$${}_0^C D_t^\alpha L_n(t;\alpha)=\sum_{k=1}^{n} D_{n,k}\left(\frac{t}{T}\right)^{(k-1)\alpha}, \quad (24)$$
$$D_{n,k}=\frac{\Gamma(1+k\alpha)}{\Gamma(1+k\alpha-\alpha)T^\alpha}C_{n,k}.$$

Noteworthy, ${}_0^C D_t^\alpha L_n(t;\alpha)\in\mathcal{M}_{n,\alpha}$ that is a valuable property in the approximation theory. We emphasis that, as n increases the coefficients $D_{n,k}$ become very large and direct calculation of ${}_0^C D_t^\alpha L_n(t;\alpha)$ can also be problematic. In the sequel, we consider a stable numerical method as the second way for evaluating of ${}_0^C D_t^\alpha L_n(t;\alpha)$.

Theorem 3.2 *Let $0<\alpha<1$ be a real number and $t\in[0,T]$. Then the representation*

$${}_0^C D_t^\alpha L_n(t;\alpha)= \quad (25)$$
$$\frac{1+n\alpha}{\alpha\Gamma(1-\alpha)T^\alpha}\int_0^1\left(1-x^{\frac{1}{\alpha}}\right)^{-\alpha}J_{n-1}^{(1,\frac{1}{\alpha})}\left(2\left(\frac{t}{T}\right)^\alpha x-1\right)dx,$$

holds true.

Proof. Consult [30]. □

$$\int_0^1\left(1-t^{\frac{1}{\alpha}}\right)^{-\alpha}f(t)dt=\sum_{k=1}^{N}w_k^{(\alpha)}f(\tau_k^{(\alpha)}), f\in\mathcal{P}_{2N}. \quad (26)$$

Clearly, the function $w(t;\alpha)=\left(1-t^{\frac{1}{\alpha}}\right)^{-\alpha}$ is a nonclassical weight function and for each value of α the Golub–Welsch algorithm explained in Section 2.3 should be used for calculating the weights $\{w_k^{(\alpha)}\}_{k=1}^N$ and nodes $\{\tau_k^{(\alpha)}\}_{k=1}^N$. Therefore, as the quadrature rule (26) for $N=[n/2]$ becomes exact, Eq. (25) is equivalent to

$${}_0^C D_t^\alpha L_n(t;\alpha)= \quad (27)$$
$$\frac{1+n\alpha}{\Gamma(1-\alpha)T^\alpha}\sum_{k=1}^{[\frac{n}{2}]}w_k^{(\alpha)}J_{n-1}^{(1,\frac{1}{\alpha})}\left(2\left(\frac{t}{T}\right)^\alpha\tau_k^{(\alpha)}-1\right).$$

4. The Müntz-Legendre PS method

In this section, we construct a novel PS method based on the Müntz-Legendre basis and Radau points for the numerical solution of nonlinear FOCPs.

4.1 Problem statement

Consider the following nonlinear FOCP in Bolza form: Minimize the performance index

$$J=\mathbf{h}\Big(t_f,\mathbf{X}(t_f)\Big)+\int_0^{t_f}\mathbf{g}\Big(t,\mathbf{X}(t),\mathbf{U}(t)\Big)dt, \quad (28)$$

subject to the fractional order system dynamics

$${}_0^C D_t^\alpha\mathbf{X}(t)=\mathbf{f}\Big(t,\mathbf{X}(t),\mathbf{U}(t)\Big),\quad t\in[0,t_f], \quad (29)$$

the initial conditions

$$\mathbf{X}(0)=\mathbf{x}_0, \quad (30)$$

https://doi.org/10.57647/ijm2c.2025.150423

and the terminal state constraints

$$\boldsymbol{\psi}\Big(t_f, \mathbf{X}(t_f)\Big) = 0, \tag{31}$$

in which t_f is the terminal time, $\mathbf{X}(t) \in \mathbb{R}^m$, $\mathbf{U}(t) \in \mathbb{R}^n$ are respectively the state and control vectors and $\mathbf{X}_0$ is a given initial state. We assume that the functions $\mathbf{f} : [0, t_f] \times \mathbb{R}^m \times \mathbb{R}^n \to \mathbb{R}^m$, $\mathbf{g} : [0, t_f] \times \mathbb{R}^m \times \mathbb{R}^n \to \mathbb{R}$, $\mathbf{h} : \mathbb{R} \times \mathbb{R}^m \to \mathbb{R}$ and $\boldsymbol{\psi} : [0, t_f] \times \mathbb{R}^m \to \mathbb{R}^m$ are continuously differentiable and the problem is controllable.

Consider now the Hamiltonian function $\mathcal{H} = \mathbf{g}(t, \mathbf{X}, \mathbf{U}) + \boldsymbol{\lambda}^T \mathbf{f}(t, \mathbf{X}, \mathbf{U})$ where the vector function $\boldsymbol{\lambda}(t)$ is called the costate. The necessary optimality conditions of the continuous-time FOCP (28)–(31) are derived using the Pontryagin Minimum Principle as

$$ {}_0^C D_t^{\alpha} \mathbf{X}(t) = \mathcal{H}_{\boldsymbol{\lambda}}, \tag{32}$$

$$\mathbf{X}(0) = \mathbf{x}_0, \tag{33}$$

$$ {}_0^C D_t^{\alpha} \boldsymbol{\lambda}(t) = -\mathcal{H}_{\mathbf{X}}, \tag{34}$$

$$\Big(\boldsymbol{\lambda}(t) - \mathbf{h}_{\mathbf{X}}(t, \mathbf{X}(t)) + \boldsymbol{\upsilon}^T \boldsymbol{\psi}_{\mathbf{X}}(t, \mathbf{X}(t))\Big)\Big|_{t_f} = 0, \tag{35}$$

$$\boldsymbol{\psi}\Big(t_f, \mathbf{X}(t_f)\Big) = 0, \tag{36}$$

$$\mathcal{H}_{\mathbf{U}} = 0. \tag{37}$$

4.2 Müntz–Legendre–Radau PS discretization

We first set $T = t_f$ and approximate the state and control functions by the shifted Müntz-Legendre polynomials as the finite sums

$$\mathbf{X}(t) \approx P^N \mathbf{X}(t) = \sum_{j=0}^{N} \mathbf{X}_j L_j(t; \alpha), \tag{38}$$

$$\mathbf{U}(t) \approx P^N \mathbf{U}(t) = \sum_{j=0}^{N} \mathbf{U}_j L_j(t; \alpha), \tag{39}$$

where $\mathbf{X}_j$ and $\mathbf{U}_j$ are totally $(N+1)(m+n)$ unknown variables to be determined.

Let $\{x_l\}_{l=0}^N$ be the Legendre–Gauss–Radau points associated with the interval $[0, t_f)$. Collocating the fractional system dynamics (29) at the $N+1$ points $\{t_l = (x_l)^{\frac{1}{\alpha}}\}_{l=0}^N$, yields

$$ {}_0^C D_t^{\alpha} \mathbf{X}(t_l) = \mathbf{f}\Big(t_l, \mathbf{X}(t_l), \mathbf{U}(t_l)\Big), \quad l = 0, \ldots, N. \tag{40}$$

Furthermore, ${}_0^C D_t^{\alpha} \mathbf{X}(t_l)$ is approximated using Eq. (27) as

$$ {}_0^C D_t^{\alpha} \mathbf{X}(t_l) \approx {}_0^C D_t^{\alpha} (P^N \mathbf{X})(t_l) = \sum_{j=0}^{N} d_{lj} \mathbf{X}_j, \tag{41}$$

where

$$d_{lj} = \frac{1 + j\alpha}{\Gamma(1-\alpha) T^{\alpha}} \sum_{k=1}^{[\frac{j}{2}]} w_k^{(\alpha)} J_{j-1}^{(1, \frac{1}{\alpha})} \left(2 \left(\frac{t_l}{T}\right)^{\alpha} \tau_k^{(\alpha)} - 1\right).$$

Substituting Eqs. (38)–(39) and (41) into Eq. (40), for $0 \leqslant l \leqslant N$ we obtain $m(N+1)$ algebraic constraints

$$\sum_{j=0}^{N} d_{lj} \mathbf{X}_j - \mathbf{f}\Big(t_l, P^N \mathbf{X}(t_l), P^N \mathbf{U}(t_l)\Big) = 0. \tag{42}$$

Moreover, approximating the initial conditions (30), gives m algebraic constraints as

$$P^N \mathbf{X}(0) - \mathbf{x}_0 = 0, \tag{43}$$

and, as $L_j(t_f; \alpha) = 1$, the terminal state constraints (31), give m algebraic constraints as

$$\boldsymbol{\psi}\Big(t_f, \sum_{j=0}^{N} \mathbf{X}_j\Big) = 0. \tag{44}$$

Finally, the cost functional is approximated by substituting Eqs. (38)–(39) into Eq. (28) and utilizing the standard Legendre-Gauss-Radau quadrature rule, to get

$$\begin{aligned} J &\simeq J_N \\ &= \mathbf{h}\Big(t_f, \sum_{j=0}^{N} \mathbf{X}_j\Big) + \sum_{l=0}^{N} \widehat{w}_l \, \mathbf{g}\Big(x_l, P^N \mathbf{X}(x_l), P^N \mathbf{U}(x_l)\Big), \end{aligned} \tag{45}$$

where $\widehat{w}_l$ and x_l are the standard Legendre-Gauss-Radau weights and nodes on the interval $[0, t_f)$, respectively.

The finite-dimensional nonlinear programming problem that emerges from the aforementioned Radau PS discretization can be succinctly summarized as follows: Minimize

$$J_N = \mathbf{h}\Big(t_f, \sum_{j=0}^{N} \mathbf{X}_j\Big) + \sum_{l=0}^{N} \widehat{w}_l \, \mathbf{g}\Big(x_l, P^N \mathbf{X}(x_l), P^N \mathbf{U}(x_l)\Big), \tag{46}$$

subject to

$$\begin{cases} P^N \mathbf{X}(0) - \mathbf{x}_0 = 0, \\ \boldsymbol{\psi}\Big(t_f, \sum_{j=0}^{N} \mathbf{X}_j\Big) = 0, \\ \sum_{j=0}^{N} d_{lj} \mathbf{X}_j - \mathbf{f}\Big(t_l, P^N \mathbf{X}(t_l), P^N \mathbf{U}(t_l)\Big) = 0, \ l = 0, 1, \ldots, N. \end{cases} \tag{47}$$

This NLP problem can be solved by a suitable globally convergent algorithm.

5. Costate estimation

In this section, we propose a novel costate estimation scheme using PS methods. The authors of [27] have developed a procedure for estimating costate utilizing PS methods, which are grounded in the relationships between the KKT multipliers of the discrete NLP and the costate, as well as the Lagrange multipliers associated with the continuous-time integer order OCP. Further, in [2], we have derived a novel costate estimation procedure based on the necessary optimality conditions for integer order OCPs. Here, we are going to extend our work in [2] to the nonlinear FOCP in Eqs. (28)–(31). To this end, consider the necessary optimality conditions (32)–(37) and let $\mathbf{X}^N(t)$ and $\mathbf{U}^N(t)$ be the obtained the approximations to $\mathbf{X}(t)$ and $\mathbf{U}(t)$ using the Müntz PS discretization of Section 4. By substituting $\mathbf{X}^N(t)$ and $\mathbf{U}^N(t)$ into Eqs. (34),(35) and (37), we obtain

$$-\mathcal{H}_{\mathbf{x}}\big|_{(\mathbf{X}^N, \mathbf{U}^N)} = {}_0^C D_t^{\alpha} \boldsymbol{\lambda}(t) = -\mathbf{g}_{\mathbf{x}}^N - \mathbf{f}_{\mathbf{x}}^N \boldsymbol{\lambda}(t), \tag{48}$$

https://doi.org/10.57647/ijm2c.2025.150423

$$\boldsymbol{\lambda}(t_f) = \mathbf{h}_{\mathbf{X}}\Big(t_f, \mathbf{X}^N(t_f)\Big) - \boldsymbol{\upsilon}^T \boldsymbol{\psi}_{\mathbf{X}}\Big(t_f, \mathbf{X}^N(t_f)\Big), \quad (49)$$

$$\mathcal{H}_{\mathrm{U}}\big|_{(\mathbf{X}^N, \mathbf{U}^N)} = 0 = \mathbf{g}_{\mathrm{U}}^N + \mathbf{f}_{\mathrm{U}}^N \boldsymbol{\lambda}(t). \quad (50)$$

Eq. (48) is a system of linear FDEs of order $0 < \alpha < 1$, Eq. (49) gives boundary conditions for the FDE (48) and Eq. (50) is a system of linear algebraic equations for the unknowns of the vector $\boldsymbol{\lambda}(t)$. Now, based on the underlying problem structure, we introduce three different schemes to approximate the costate, $\boldsymbol{\lambda}^N(t)$.

- **Scheme A**: Consider the case $\boldsymbol{\psi}_{\mathbf{X}}\Big(t_f, \mathbf{X}^N(t_f)\Big) = 0$. In this case, there is no need to obtain the multipliers $\boldsymbol{\upsilon}$; hence, our first scheme for costate estimation is to utilize the Müntz collocation method to solve the system of linear FDEs (48) with the boundary conditions (49).

- **Scheme B**: Suppose that $\boldsymbol{\psi}_{\mathbf{X}}\Big(t_f, \mathbf{X}^N(t_f)\Big) \neq 0$ and $m = n$, so the boundary condition (49) is not usable. In this case, we obtain the approximations $\boldsymbol{\lambda}^N(t)$, by solving the system of linear algebraic equations (50).

- **Scheme C**: Suppose that $\boldsymbol{\psi}_{\mathbf{X}}\Big(t_f, \mathbf{X}^N(t_f)\Big) \neq 0$ and $m \neq n$. Since we have assumed that the underlying FOCP is controllable, Eq. (50) gives a full rank linear system of algebraic equations. In this case, if $m > n$ then, n out of m functions $\lambda_j(t)$ are derived using Eq. (50), while the remaining $m - n$ functions are derived using Eq. (48) with the initial conditions $\mathbf{g}_{\mathrm{U}}^N + \mathbf{f}_{\mathrm{U}}^N \boldsymbol{\lambda}(0) = 0$. Otherwise, the vector function $\boldsymbol{\lambda}(t)$ is derived using Eq. (50).

6. Illustrative examples

In this section three examples are solved to illustrate the efficiency and accuracy of the presented Muntz PS method and costate estimation schemes. Whenever we have the exact solutions, we use the below accuracy criterions:

$$E_J = |J_N - J^*|,$$
$$E_{\mathbf{X}} = \left\|\mathbf{X}^N(t) - \mathbf{X}^*(t)\right\|_{L^\infty(I)},$$
$$E_{\mathbf{U}} = \left\|\mathbf{U}^N(t) - \mathbf{U}^*(t)\right\|_{L^\infty(I)},$$
$$E_{\boldsymbol{\lambda}} = \left\|\boldsymbol{\lambda}^N(t) - \boldsymbol{\lambda}^*(t)\right\|_{L^\infty(I)}.$$

Furthermore, for assessing the accuracy when the exact solution is unavailable, our accuracy criterions are as follows. By substituting $\mathbf{U}^N$ into Eq. (29), a system of nonlinear FDEs is obtained as an accuracy criterion for the fractional system dynamics:

$${}_0^C D_t^\alpha \mathbf{X}(t) = \mathbf{f}\Big(t, \mathbf{X}(t), \mathbf{U}^N(t)\Big), \quad \mathbf{X}(0) = \mathbf{x}_0. \quad (51)$$

To solve (51), we have utilized the Müntz collocation method to obtain the approximate solution $\widetilde{\mathbf{X}}(t)$. Then we define

$$\varepsilon_{dyn} = \left\|\widetilde{\mathbf{X}}(t) - \mathbf{X}^N(t)\right\|_{L^\infty(I)}.$$

Moreover, let $\boldsymbol{\lambda}^{N,s}(t)$, $s = A, B, C$ be the costate estimations obtained using the schemes A, B and C of Section 5. Then, we define the accuracy criterions for costate estimation as

$$\varepsilon_{\mathcal{H}_{\mathbf{X}}} = \max_{s\in\{A,B,C\}} \left\{\left\|{}_0^C D_t^\alpha \boldsymbol{\lambda}^{N,s} + \mathcal{H}_{\mathbf{X}}\right\|_{L^\infty(I)}\right\},$$

$$\varepsilon_{\mathcal{H}_{\mathrm{U}}} = \max_{s\in\{A,B,C\}} \left\{\left\|\mathcal{H}_{\mathrm{U}}\right\|_{L^\infty(I)}\right\}.$$

Example 6.1 As the first example, consider the following linear-quadratic FOCP of minimizing the cost functional [12],

$$J = \int_0^1 \left(\Big(x(t) - t^{3\alpha}\Big)^2 + \left(u(t) + \frac{t^\alpha}{\Gamma(\alpha+3)} - \frac{\Gamma(3\alpha+1)}{\Gamma(2\alpha+1)}\right)^2\right) dt,$$

with the fractional state equation,

$${}_0^C D_t^\alpha x(t) = \frac{x(t)}{\Gamma(\alpha+3)} + t^{2\alpha} u(t),$$

and the initial condition

$$x(0) = 0.$$

The exact solution to this problem is

$$x^*(t) = t^{3\alpha},$$
$$u^*(t) = -\frac{t^\alpha}{\Gamma(\alpha+3)} + \left(\frac{\Gamma(3\alpha+1)}{\Gamma(2\alpha+1)}\right),$$
$$\lambda^*(t) = 0.$$

Since the exact solution is available, in Table 1 and Table 2 we have reported the errors E_x and E_u and compared our results with the variational iteration method (VIM) and the modified Adomian decomposition method (MADM) presented in [12]. It is seen that our method is more accurate. For costate estimation, we first consider the Hamiltonian function as

$$\mathcal{H} = \Big(x(t) - t^{3\alpha}\Big)^2 + \left(u(t) + \frac{t^\alpha}{\Gamma(\alpha+3)} - \frac{\Gamma(3\alpha+1)}{\Gamma(2\alpha+1)}\right)^2 + \lambda(t)\left(\frac{x(t)}{\Gamma(\alpha+3)} + t^{2\alpha}u(t)\right).$$

Then, using Eqs. (48)–(50) evaluated at $x^N(t)$ and $u^N(t)$, we obtain

$${}_0^C D_t^\alpha \lambda(t) + \frac{1}{\Gamma(\alpha+3)}\lambda(t) + 2\Big(x^N(t) - t^{3\alpha}\Big) = 0, \quad (52)$$
$$\lambda(1) = 0,$$

$$2\left(u^N(t) + \frac{t^\alpha}{\Gamma(\alpha+3)} - \frac{\Gamma(3\alpha+1)}{\Gamma(2\alpha+1)}\right) + t^{2\alpha}\lambda(t) = 0. \quad (53)$$

In this problem, we have $m = n = 1$ and according to **Scheme A**, we solve the linear FDE (52) to estimate $\lambda(t)$. Note that, estimating $\lambda(t)$ using (53) is numerically problematic at $t = 0$ (**Scheme B**). In Fig. 1, the approximations of the optimal state and control and the costate obtained using the present method for $N = 15$ and various values of α are depicted. As $\lambda^*(t) = 0$, Fig. 1 also shows the error in costate estimations.

https://doi.org/10.57647/ijm2c.2025.150423

Table 1. Absolute errors E_x at $\alpha = 0.7$ for Example 6.1.

	Present method		VIM [12]	
t	$N = 5$	$N = 10$	$N = 5$	$N = 10$
0.1	4.8398×10^{-7}	5.1486×10^{-18}	2.9864×10^{-6}	1.0408×10^{-17}
0.2	1.7208×10^{-6}	3.6359×10^{-17}	2.3475×10^{-5}	8.3960×10^{-16}
0.3	1.8873×10^{-5}	1.2351×10^{-17}	7.8174×10^{-5}	4.5852×10^{-14}
0.4	6.4392×10^{-5}	2.9143×10^{-16}	1.8321×10^{-4}	1.3341×10^{-12}
0.5	7.6605×10^{-5}	4.5519×10^{-16}	3.5361×10^{-4}	2.6890×10^{-11}
0.6	3.3861×10^{-5}	1.2767×10^{-15}	6.0057×10^{-4}	4.0799×10^{-10}
0.7	1.0880×10^{-4}	9.8809×10^{-15}	9.2314×10^{-4}	4.8369×10^{-9}
0.8	7.6605×10^{-4}	4.5692×10^{-14}	1.2881×10^{-3}	4.6087×10^{-8}
0.9	9.8809×10^{-4}	7.6225×10^{-15}	1.5878×10^{-3}	3.6218×10^{-7}

Table 2. Absolute errors E_u at $\alpha = 0.6$ for Example 6.1.

	Present method		MADM [12]	
t	$N = 5$	$N = 15$	$N = 5$	$N = 15$
0.1	7.5495×10^{-5}	1.0214×10^{-11}	1.0764×10^{-3}	3.8564×10^{-9}
0.2	6.8833×10^{-5}	1.2434×10^{-11}	1.2911×10^{-3}	7.6381×10^{-9}
0.3	5.1070×10^{-5}	5.2156×10^{-11}	1.5287×10^{-3}	1.1142×10^{-8}
0.4	4.2188×10^{-5}	4.6629×10^{-10}	1.7755×10^{-3}	1.5208×10^{-8}
0.5	3.3306×10^{-5}	8.4376×10^{-10}	2.0031×10^{-3}	1.8998×10^{-8}
0.6	1.3322×10^{-5}	1.0214×10^{-9}	2.1615×10^{-3}	2.2791×10^{-8}
0.7	1.0880×10^{-5}	3.3306×10^{-9}	2.1737×10^{-3}	2.6581×10^{-8}
0.8	3.7747×10^{-5}	6.6613×10^{-9}	1.9278×10^{-3}	2.0361×10^{-8}
0.9	9.8809×10^{-5}	1.9984×10^{-9}	1.2705×10^{-3}	3.4086×10^{-8}

Example 6.2 Consider minimizing the following cost functional

$$J = \int_0^1 \Big(x_1^2(t) + u^2(t)\Big)dt,$$

subject to the nonlinear and coupled state equations

$$\begin{aligned} &{}_0^C D_t^\alpha x_1(t) = x_2(t),\\ &{}_0^C D_t^\alpha x_2(t) = -x_1(t) + 1.4x_2(t) - 0.14x_2^3(t) + 4u(t), \end{aligned}$$

and initial conditions

$$x_1(0) = -5, \qquad x_2(0) = -5.$$

This problem for $\alpha = 1$ is the manual of PROPT, which is called Rayleigh [14]. For costate estimation, we consider the Hamiltonian function as

$$\begin{aligned} \mathcal{H} \;=\; & x_1^2(t) + u^2(t) + \lambda_1(t)x_2(t)\\ & +\lambda_2(t)\Big(-x_1(t) + 1.4x_2(t) - 0.14x_2^3(t) + 4u(t)\Big). \end{aligned}$$

Then, using Eqs. (48)–(50) evaluated at x_1^N, x_2^N and u^N, we get

$${}_0^C D_t^\alpha \lambda_1(t) - \lambda_2(t) + 2x_1^N(t) = 0, \qquad \lambda_1(1) = 0, \quad (54)$$

$${}_0^C D_t^\alpha \lambda_2(t) + \lambda_1(t) - \Big(0.42x_2^{N^2}(t) - 1.4\Big)\lambda_2(t) = 0, \quad (55)$$
$$\lambda_2(1) = 0,$$

$$u^N(t) + 2\lambda_2(t) = 0. \quad (56)$$

According to **Scheme A**, we can solve the system of linear FDEs (54)–(55). Further, according to **Scheme C**, we should first estimate $\lambda_2(t)$ by using (56) and then solve the linear FDE (54) to estimate $\lambda_1(t)$. However, our numerical study revealed that in this example, **Scheme A** provides more accurate results.

The approximations of the optimal states and control and the costates obtained for $\alpha = 0.8, 0.9, 1$ and $N = 15$ are displayed in Fig. 2. Moreover, the obtained numerical results of the cost functional J for $\alpha = 08, 0.9, 1$ and several values of N are reported in Table 3 that demonstrate the convergence and spectral accuracy of the proposed method.

Example 6.3 Recently, a fractional optimal control modeling with Caputo derivative has been presented for tumor burden under immune suppression [22]. If we consider t as time, $T(t)$ as tumor cells, $I(t)$ as immune cells, $\widetilde{N}(t)$ as normal cells, $F(t)$ as fat cells and $\widetilde{D}(t)$ as chemotherapeutic drugs, then the following cancer model describes the interactions between $T(t)$, $I(t)$, $\widetilde{N}(t)$ and $F(t)$ at time t near tumor site, while $\widetilde{D}(t)$ is injected into the body:

$$\text{Min} \quad J = \int_0^1 \Big(\omega_1 T(t) - \omega_2 \widetilde{N}(t) + \omega_3 u^2(t)\Big)dt,$$

https://doi.org/10.57647/ijm2c.2025.150423

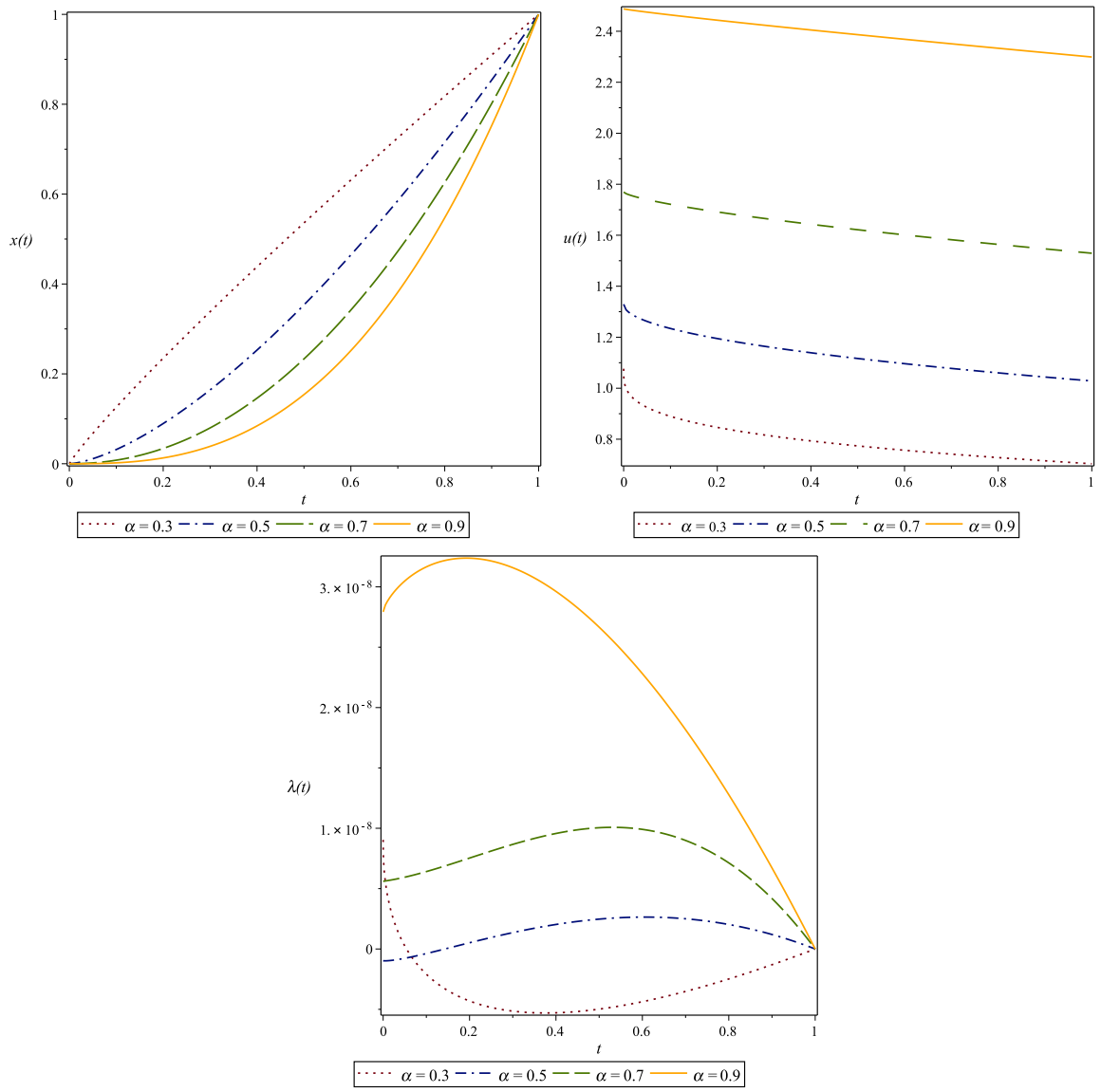

Figure 1. Approximations of state, control and costate for Example 6.1 for $N = 15$ and different values of α.

subject to the following fractional dynamical system

$$\begin{aligned}
{}_0^C D_t^\alpha T(t) &= r_1 T(t)\Big(1 - p_1 T(t)\Big) - a_1 T(t) I(t) \\
&\quad - a_2 T(t)\widetilde{N}(t) + c_1 T(t) F(t) - \gamma_1 \widetilde{D}(t) T(t), \\
{}_0^C D_t^\alpha I(t) &= s_1 + b_1 \frac{T(t) I(t)}{h + T(t)} - a_3 T(t) I(t) - \mu_1 I(t) \\
&\quad - \gamma_2 \widetilde{D}(t) I(t), \\
{}_0^C D_t^\alpha \widetilde{N}(t) &= r_2 \widetilde{N}(t)\left(1 - p_2 \widetilde{N}(t)\right) - a_4 T(t)\widetilde{N}(t) \\
&\quad - \gamma_3 \widetilde{D}(t)\widetilde{N}(t), \\
{}_0^C D_t^\alpha F(t) &= r_3 F(t)\Big(1 - p_3 F(t)\Big) - a_5 T(t) F(t) \\
&\quad - \gamma_4 \widetilde{D}(t) F(t), \\
{}_0^C D_t^\alpha \widetilde{D}(t) &= u(t) - \zeta \widetilde{D}(t),
\end{aligned}$$

and initial conditions

$$\begin{aligned}
&T(0) = 1, \quad I(0) = 0.001, \quad F(0) = 4, \\
&\widetilde{N}(0) = 0.25, \quad \widetilde{D}(0) = 0.5,
\end{aligned}$$

note that, $u(t)$ is the dose of injection to be controlled. We consider the values of the weights as $\omega_1 = 20$, $\omega_2 = 1$ and $\omega_3 = 1$ and the values of other parameters are given in Table 4. *We solved this FOCP using the Müntz PS method of Section 4 and the costate estimation schemes of Section 5. In this problem, Eqs. (48)–(50) evaluated at $T^N(t)$, $I^N(t)$, $\widetilde{N}^N(t)$, $F^N(t)$, $\widetilde{D}^N(t)$ and $u^N(t)$, read*

$$\begin{aligned}
&{}_0^C D_t^\alpha \lambda_1(t) + \omega_1 + \lambda_1(t)\Big(r_1 - 2r_1 p_1 T^N(t) + c_1 F^N(t) \\
&- a_1 I^N(t) - a_2 \widetilde{N}^N(t) - \gamma_1 \widetilde{D}^N(t)\Big) + \lambda_2(t)\Big(\frac{b_1 I^N(t)}{h + T^N(t)} \\
&- \frac{b_1 T^N(t) I^N(t)}{(h + T^N(t))^2} - a_3 I^N(t)\Big) - a_4 \lambda_3(t)\widetilde{N}^N(t) \\
&- a_5 \lambda_4(t) F^N(t) = 0, \qquad (57)
\end{aligned}$$

$$\begin{aligned}
&{}_0^C D_t^\alpha \lambda_2(t) - a_1 \lambda_1(t) T^N(t) + \lambda_2(t)\Big(\frac{b_1 T^N(t)}{h + T^N(t)} \\
&- a_3 T^N(t) - \gamma_2 \widetilde{D}^N(t) - \mu_1\Big) = 0, \qquad (58)
\end{aligned}$$

https://doi.org/10.57647/ijm2c.2025.150423

Table 3. Approximate values of J and costate estimation for different α for Example 6.2.

N	J_N	ε_{dyn}	$\varepsilon_{\mathcal{H}x}$	$\varepsilon_{\mathcal{H}u}$
$\alpha = 0.8$				
7	20.910	7.86×10^{-6}	2.68×10^{-1}	1.16×10^{-2}
9	20.900	3.22×10^{-6}	2.83×10^{-1}	1.15×10^{-2}
11	20.8991	7.93×10^{-7}	2.99×10^{-1}	1.13×10^{-2}
13	20.898843	1.15×10^{-7}	3.14×10^{-1}	1.13×10^{-2}
15	20.898838	7.93×10^{-8}	3.27×10^{-1}	1.13×10^{-2}
$\alpha = 0.9$				
7	23.89	1.42×10^{-6}	1.21×10^{-1}	4.96×10^{-2}
9	23.8844	4.12×10^{-7}	1.32×10^{-1}	4.84×10^{-2}
11	23.88418	2.23×10^{-7}	1.41×10^{-1}	4.80×10^{-2}
13	23.88391	1.32×10^{-7}	1.50×10^{-1}	4.84×10^{-2}
15	23.883898	4.12×10^{-8}	1.57×10^{-1}	4.84×10^{-2}
$\alpha = 1$				
7	26.827	6.09×10^{-7}	2.28×10^{-2}	2.53×10^{-4}
9	26.824	1.43×10^{-7}	2.28×10^{-2}	8.38×10^{-4}
11	26.8240	1.24×10^{-7}	2.72×10^{-2}	8.35×10^{-4}
13	26.8237499	6.11×10^{-8}	2.89×10^{-2}	8.39×10^{-4}
15	26.8237492	4.43×10^{-8}	3.04×10^{-2}	8.34×10^{-4}

Table 4. Values of the parameters for the FOC cancer model in Example 6.3.

	Description	Units	Estimate value
r_1	Growth rate of tumor cells	day^{-1}	1.5
r_2	Growth rate of tumor cells	day^{-1}	1
r_3	Growth rate of tumor cells	day^{-1}	0.75
p_1	Reciprocal carrying capacity of tumor cells	$cells^{-1}$	1
p_2	Reciprocal carrying capacity of tumor cells	$cells^{-1}$	1
p_3	Reciprocal carrying capacity of tumor cells	$cells^{-1}$	1.5
a_1	Competition term of tumor cells with immune cells	$cells^{-1}day^{-1}$	0.5
a_2	Competition term of tumor cells with immune cells	$cells^{-1}day^{-1}$	1
a_3	Competition term of tumor cells with immune cells	$cells^{-1}day^{-1}$	0.5
a_4	Competition term of tumor cells with immune cells	$cells^{-1}day^{-1}$	1
a_5	Competition term of tumor cells with immune cells	$cells^{-1}day^{-1}$	0.1
$c1$	Competition term of fat cells with tumor cells	$cells^{-1}day^{-1}$	1.5
γ_1	Response of tumor cells to chemotherapeutic drug	day^{-1}	0.08
γ_2	Response of tumor cells to chemotherapeutic drug	day^{-1}	2×10^{-11}
γ_3	Response of tumor cells to chemotherapeutic drug	day^{-1}	0.008
γ_4	Response of tumor cells to chemotherapeutic drug	day^{-1}	0.008
s_1	Immune source rate	$cells^{-1}day^{-1}$	0.33
b_1	Recruitment rate of immune cells by tumor cells	day^{-1}	0.01
h	Immune response stimulated by tumor cells	$cells^2$	0.3
μ_1	Death rate of immune cells	day^{-1}	0.2
ζ	Decay rate of $\widetilde{D}$	day^{-1}	0.1

$$ {}_0^C D_t^\alpha \lambda_3(t) - a_2\lambda_1(t)T^N(t) + \lambda_3(t)\Big(r_2 - 2r_2p_2\widetilde{N}^N(t) - a_4T^N(t) - \gamma_3\widetilde{D}^N(t)\Big) - \omega_2 = 0, \tag{59} $$

$$ {}_0^C D_t^\alpha \lambda_4(t) + c_1\lambda_1(t)T^N(t) + \lambda_4(t)\Big(r_3 - 2r_3p_3F^N(t) - a_5T^N(t) - \gamma_4\widetilde{D}^N(t)\Big) = 0, \tag{60} $$

$$ {}_0^C D_t^\alpha \lambda_5(t) - \Big(\gamma_1\lambda_1(t)T^N(t) + \gamma_2\lambda_2(t)I^N(t) + \gamma_3\lambda_3(t)\widetilde{N}^N(t) + \gamma_4\lambda_4(t)F^N(t) + \zeta\lambda_5(t)\Big) = 0, \tag{61} $$

$$ \lambda_1(1) = 0, \quad \lambda_2(1) = 0, \quad \lambda_3(1) = 0, $$
$$ \lambda_4(1) = 0, \quad \lambda_5(1) = 0, \tag{62} $$

$$ \lambda_5(t) + 2\omega_3u^N(t) = 0. \tag{63} $$

Here, we have $m > n$ and for costate estimation we can utilize Scheme A or Scheme C of Section 5. Based on

https://doi.org/10.57647/ijm2c.2025.150423

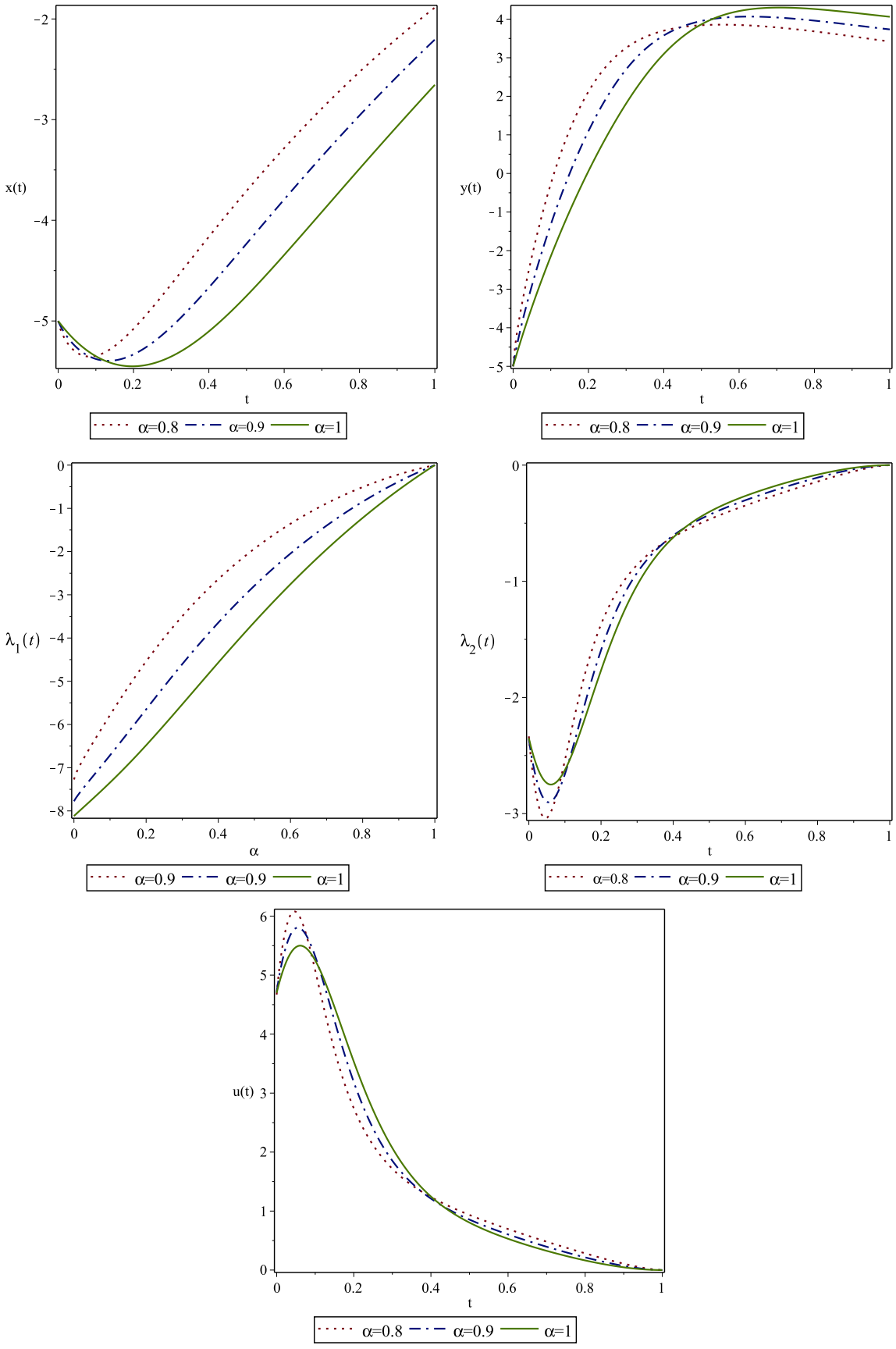

Figure 2. Approximate states, control and costates for Example 6.2 with $N = 15$.

Scheme A, we solve the system of linear FDEs (57)–(61) with the boundary conditions (62). Moreover, based on **Scheme C**, we can first estimate $\lambda_5(t)$ from (63), and then solve the linear FDEs (57)–(61) for estimating the

Table 5. Computational results of J and costate estimation errors for $\alpha = 0.8, 0.9, 1$ and various alues of N for Example 6.3.

N	J_N	ε_{dyn}	$\varepsilon_{\mathcal{H}_{\mathbf{x}}}$	$\varepsilon_{\mathcal{H}u}$
$\alpha = 0.8$				
5	9.43	2.76×10^{-3}	3.28×10^{-1}	4.33×10^{-1}
10	9.556	4.59×10^{-5}	4.08×10^{-2}	9.64×10^{-2}
15	9.55443	1.96×10^{-6}	1.56×10^{-2}	8.25×10^{-2}
20	9.5544684	5.19×10^{-7}	6.16×10^{-3}	4.16×10^{-2}
25	9.5544681	2.74×10^{-7}	8.73×10^{-4}	5.58×10^{-3}
$\alpha = 0.9$				
5	9.35	3.48×10^{-3}	1.76×10^{-1}	2.30×10^{-1}
10	9.4369	1.39×10^{-5}	3.43×10^{-2}	2.28×10^{-2}
15	9.43610	8.76×10^{-6}	4.29×10^{-3}	2.97×10^{-2}
20	9.4360997	3.80×10^{-6}	9.34×10^{-3}	2.30×10^{-3}
25	9.4360995	8.17×10^{-7}	7.10×10^{-4}	1.06×10^{-3}
$\alpha = 1$				
5	9.24	1.91×10^{-3}	1.91×10^{-3}	2.38×10^{-3}
10	9.288	1.49×10^{-6}	7.42×10^{-3}	9.23×10^{-3}
15	9.287905	6.80×10^{-7}	2.35×10^{-3}	6.54×10^{-3}
20	9.28790775	3.41×10^{-7}	6.27×10^{-4}	2.58×10^{-3}
25	9.28790773	2.11×10^{-7}	3.78×10^{-4}	7.41×10^{-4}

remaining costates $\{\lambda_i(t)\}_{i=1}^{4}$. Nonetheless, our experimental study showed that **Scheme A** provides much more accurate results. Table 5, gives the approximations of performance index J and errors $\varepsilon_{\mathcal{H}_{\mathbf{x}}}$ and $\varepsilon_{\mathcal{H}u}$ (related to **Scheme A**) for different values α and N. The spectral accuracy of the proposed method is apparent from Table 5. In Fig. 3, the graphs of approximated state variables and the control variable are plotted for different values of α and $N = 15$ and in Fig. 4, the graphs of approximated costate variables are depicted. Based on the obtained numerical results, we have the following observations: for all the considered values α, the population of tumors diminishes while the population of normal cells is replenished as a function of time. Additionally, the population of immune cells and the quantity of fat cells increase over time. Furthermore, after the passage of half the designated time and the elimination of a significant portion of the tumor population, the drug concentration $\widetilde{D}(t)$ and the dosage $u(t)$ decline.

7. Conclusion

In this article, the PS method has been utilized for the numerical resolution of a specific category of FOCPs. A distinct family of the Müntz–Legendre polynomials served as the approximation basis. The introduced PS method is noted for its simplicity, efficiency, and high precision, making it easily implementable. Additionally, a novel procedure for costate estimation was developed based on the necessary optimality conditions. The accuracy and validity of the proposed method were validated through numerical simulations across several examples including a tumor burden under immune suppression model. A potential avenue for future research would involve extending the proposed method to encompass other categories of FOCPs and FOCPs that incorporate time-delay.

Authors contributions
All the authors have participated sufficiently in the intellectual content, conception and design of this work or the analysis and interpretation of the data (when applicable), as well as the writing of the manuscript.
Availability of data and materials
The data that support the findings of this study are available from the corresponding author, upon reasonable request.

Conflict of interests
The author states that there is no conflict of interest.

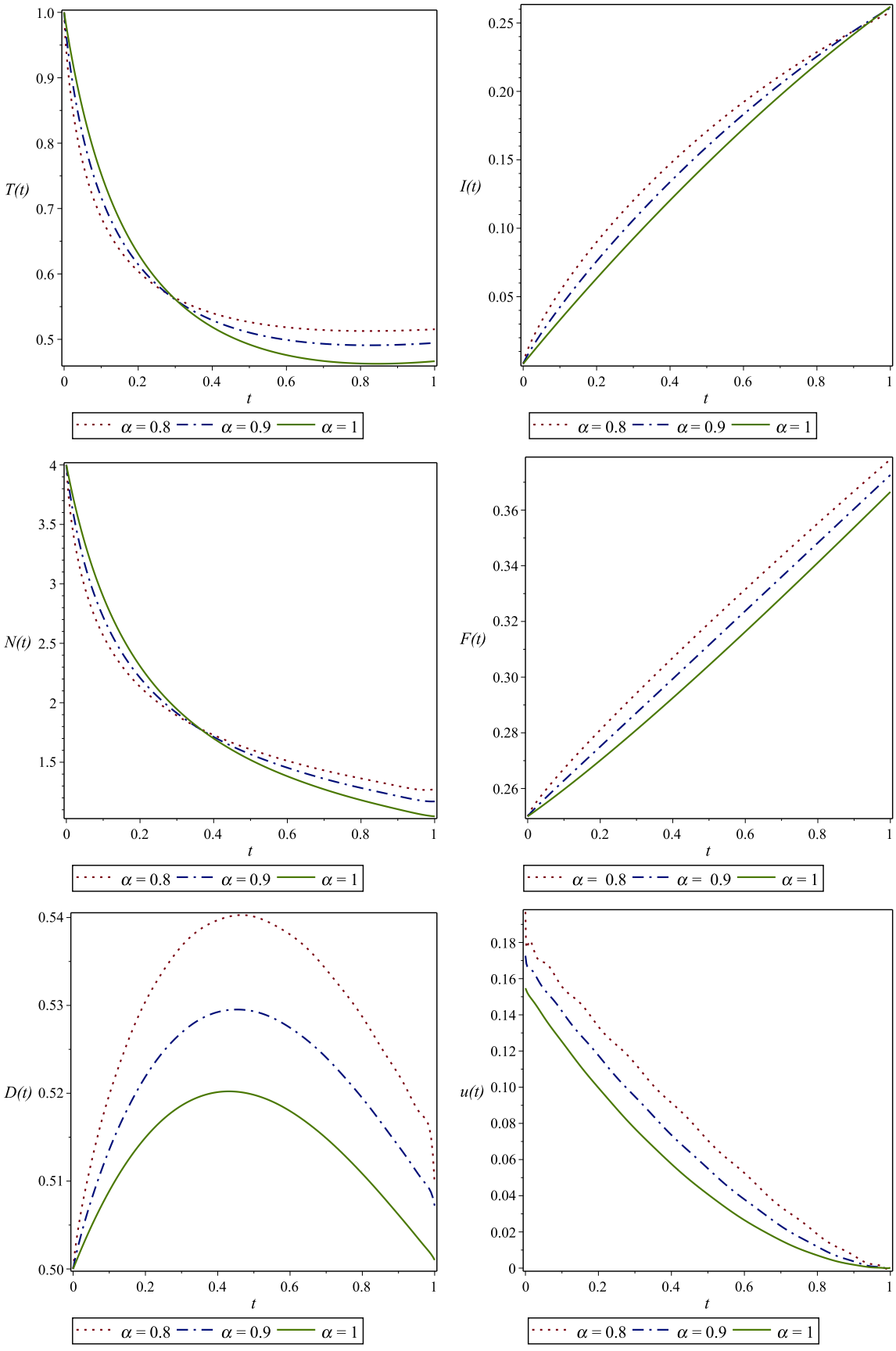

Figure 3. Approximate states and control for Example 6.3 with $N = 15$ and different values of α.

https://doi.org/10.57647/ijm2c.2025.150423

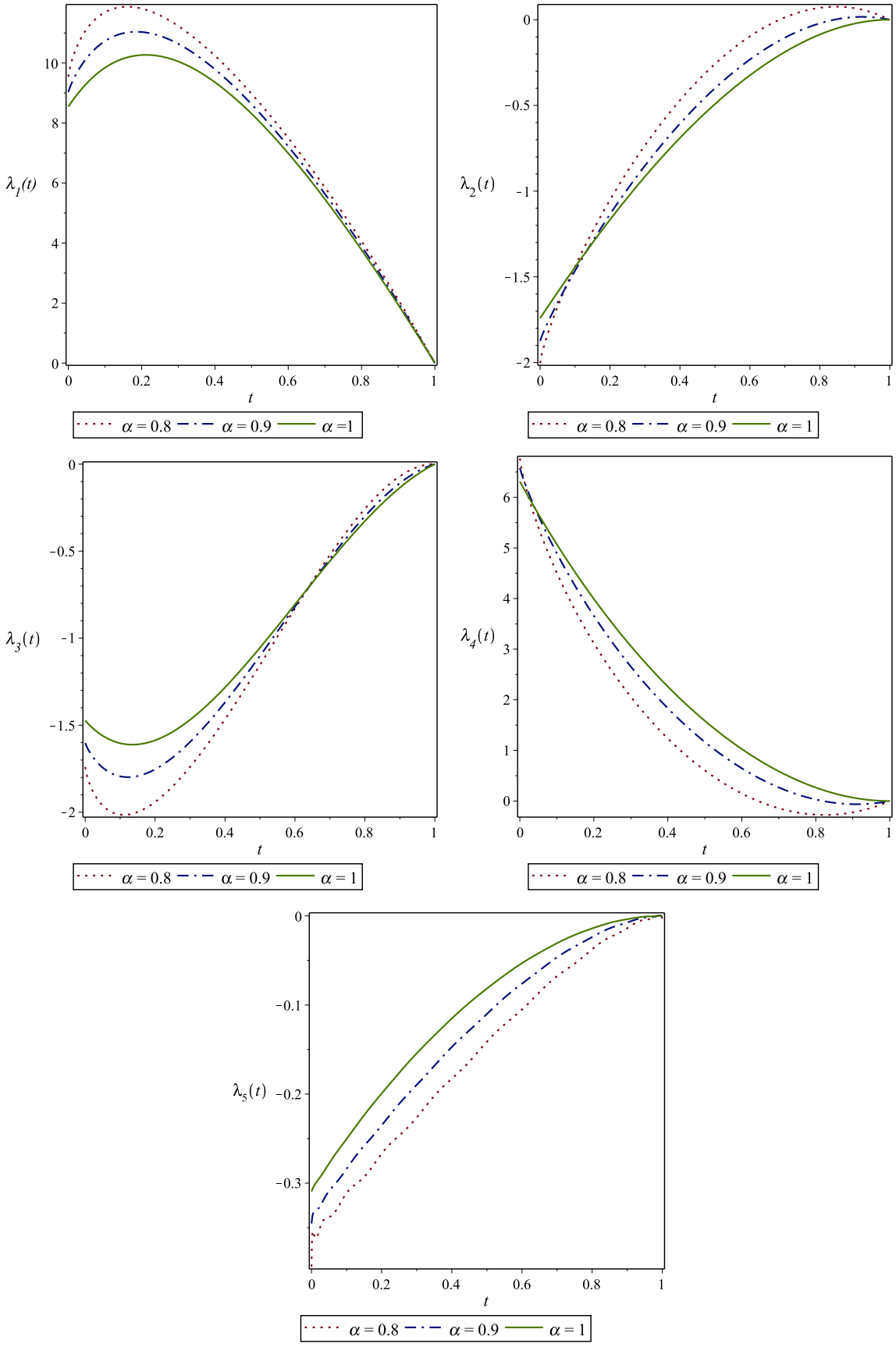

Figure 4. Approximate costates for Example 6.3 with $N = 15$ and different values of α.

https://doi.org/10.57647/ijm2c.2025.150423

References

[1] Ross IM, Karpenko M. A review of pseudospectral optimal control: from theory to flight. *Annu Rev Control*. 2012;36(2):182–197.

[2] Ghassemi H, Maleki M, Allame M. On the modification and convergence of unconstrained optimal control using pseudospectral methods. *Optim Control Appl Meth*. 2021;42(3):717–743.

[3] Tang X, Liu Z, Wang X. Integral fractional pseudospectral methods for solving fractional optimal control problems. *Automatica*. 2015;62:304–311.

[4] Ejlali N, Hosseini SM. A pseudospectral method for fractional optimal control problems. *J Optim Theory Appl*. 2017;174:83–107.

[5] Li S, Zhou Z. Legendre pseudo-spectral method for optimal control problem governed by a time-fractional diffusion equation. *Int J Comput Math*. 2018;95(6-7):1308–1325.

[6] Habibli M, Noori Skandari MH. Fractional Chebyshev pseudospectral method for fractional optimal control problems. *Optim Control Appl Meth*. 2019;40(3):558–572.

[7] Yang Y, Noori Skandari MH. Pseudospectral method for fractional infinite horizon optimal control problems. *Optim Control Appl Meth*. 2020;41(6):2201–2212.

[8] Elgindy KT. Fourier-Gegenbauer pseudospectral method for solving periodic fractional optimal control problems. *arXiv*:2304.04454v6 [math.OC]. https://doi.org/10.48550/arXiv.2304.04454

[9] Sweilam NH, Al-Ajami TM, Hoppe RHW. Numerical solution of some types of fractional optimal control problems. *Sci World J*. 2013;2013:306237. https://doi.org/10.1155/2013/306237

[10] Shafiof SM, Askari J, Shams Solary M. A numerical solution of fractional optimal control problems using spectral method and hybrid functions. *Control Optim Appl Math*. 2018;3(1):1–25.

[11] Alizadeh A, Effati S. An iterative approach for solving fractional optimal control problems. *J Vib Control*. 2016;22(8):1–19.

[12] Alizadeh A, Effati S, Heydari A. Numerical schemes for fractional optimal control problems. *J Dyn Syst Meas Control*. 2017;139(8):081011. https://doi.org/10.1115/1.4036359

[13] Akbarian T, Keyanpour M. A New approach to the numerical solution of fractional order optimal control problems. *Appl Appl Math*. 2013;8(2):523–534.

[14] Alipour M, Rostamy D, Baleanu D. Solving multi-dimensional fractional optimal control problems with inequality constraint by Bernstein polynomials operational matrices. *J Vib Control*. 2013;19(16):2523–2540. https://doi.org/10.1177/1077546312464210

[15] Lotfi A, Yousefi SA. Epsilon-Ritz method for solving a class of fractional constrained optimization problems. *J Optim Theory Appl*. 2014;163(3):884–899. https://doi.org/10.1007/s10957-013-0480-8

[16] Zeid SS, Yousefi M. Approximated solutions of linear quadratic fractional optimal control problems. *JAMSI*. 2016;12(2):83–94.

[17] Yang Y, Zhang J, Liu H, Vasilev AO. An indirect convergent Jacobi spectral collocation method for fractional optimal control problems. *Math Meth Appl Sci*. 2021;44(4):2806–2824. https://doi.org/10.1002/mma.6935

[18] Ghaderi S, Effati S, Heydari A. A new numerical approach for solving fractional optimal control problems with the Caputo–Fabrizio fractional operator. *J Math*. 2022;2022:6680319. https://doi.org/10.1155/2022/6680319

[19] Pirouzeh Z, Noori Skandari MH, Nassiri Pirbazari K. A convergent Legendre spectral collocation method for the variable-order fractional-functional optimal control problems. *J Math*. 2024;2024:3934093. https://doi.org/10.1155/2024/3934093

[20] Kheiri H, Jafari M. Fractional optimal control of an HIV/AIDS epidemic model with random testing and contact tracing. *J Appl Math Comput*. 2019;60(1-2):387–411. https://doi.org/10.1007/s12190-018-01218-x

[21] Vellappandi M, Kumar P, Govindaraj V, Albalawi W. An optimal control problem for Mosaic disease via Caputo fractional derivative. *Alexandria Eng J*. 2022;61(10):8027–8037. https://doi.org/10.1016/j.aej.2022.01.043

[22] Sweilam NH, AL-Mekhlafi SM. Optimal control for a nonlinear mathematical model of tumor under immune suppression: a numerical approach. *Optim Control Appl Meth*. 2018;39(5):1581–1596. https://doi.org/10.1002/oca.2433

[23] Cheneke KR, Rao KP, Edessa GK. Fractional derivative and optimal control analysis of Cholera epidemic model. *J Math*. 2022;2022:9075917. https://doi.org/10.1155/2022/9075917

[24] Nadeem M, Habib M, Safdar M, Mwanakatwe PK. Analysis of Climatic model using fractional optimal control. *J Math*. 2023;2023:7482381. https://doi.org/10.1155/2023/7482381

[25] Ganeshan D, Darne LJ. Optimal control of hand, foot and mouth disease model using variational iteration method. *Int J Math Model Comput*. 2018;8(4):239–254.

[26] Wameko M. Mathematical model for transmission dynamics of hepatitus C virus with optimal control strategies. *Int J Math Model Comput*. 2019;9(3):213–237.

[27] Fahroo F, Ross IM. Costate estimation by a Legendre pseudospectral method. *J Guid Control Dyn*. 2002;24(2):270–277. https://doi.org/10.2514/2.4906

[28] Benson DA, Huntington GT, Thorvaldsen TP, Rao AV. Direct trajectory optimization and costate estimation via an orthogonal collocation method. *J Guid Control Dyn*. 2006;29(6):1435–1440. https://doi.org/10.2514/1.20478

[29] Chen S, Shen J, Wang LL. Generalized Jacobi functions and their applications to fractional differential equations. *Math Comp*. 2016;85(300):1603–1638. https://doi.org/10.1090/mcom/3054

[30] Esmaeili S, Shamsi M, Luchko Y. Numerical solution of fractional differential equations with a collocation method based on Müntz polynomials. *Comput Math Appl*. 2011;62(3):918–929.

[31] Sadeghi B, Maleki M, Almasieh H. Space-time Müntz spectral collocation approach for parabolic Volterra integro-differential equations with a singular kernel. *J Nonlinear Anal Appl*. 2022;2022(1):1–10.

[32] Gautschi W. *Orthogonal Polynomials: Computation and Approximation*. Oxford University Press; 2004.

[33] Canuto C, Hussaini MY, Quarteroni A, Zang TA. *Spectral Methods: Fundamentals in Single Domains*. Springer; 2006.

[34] Golub GH, Welsch JH. Calculation of Gauss quadrature rules. *Math Comp*. 1969;23(106):221–230.

[35] Podlubny I. *Fractional Differential Equations*. Academic Press; 1999.

[36] Borwein P, Erdélyi T, Zhang J. Müntz systems and orthogonal Müntz–Legendre polynomials. *Trans Amer Math Soc*. 1994;342(2):523–542.

[37] Milovanović GV. Müntz orthogonal polynomials and their numerical evaluation. In: *Applications and Computation of Orthogonal Polynomials*. Birkhäuser Basel; 1999. p. 179–194.